PCCP

Accepted Manuscript

ROYAL SOCIETY OF CHEMISTRY

www.rsc.org/pccp

Journal Name

ARTICLE

Selective synthesis of TiO_2 single nanocrystal and titanate nanotubes: a controllable atomic arrangement approach via NH_4TiOF_3 mesocrystals

Received 00th January 20xx,
Accepted 00th January 20xx

DOI: 10.1039/x0xx00000x

www.rsc.org/

Penghua Wang,‡[a] Qiuying Yi,‡[a] Mingyang Xing,*[a] and Jinlong Zhang*[a]

The nanostructured titania and titanate have been considered as the very important materials used in the photocatalysis, photovoltaics, gas sensing and other electronic industries. In principle, the common structural feature determines that the precursor phase involving TiO_6 octahedra or similar building units may be converted to any of the nanostructured titania and titanate forms in a controllable way. Based on the atomic arrangement of ionic liquid-mediated NH_4TiOF_3 mesocrystals, TiO_2 nanocrystals and titanate nanotubes were selectively obtained in H_3BO_3 and NaOH media, respectively, by using a simple hydrothermal method. Interestingly, the titanate nanotubes were successfully formed by extraction of NH_4^+ and F from NH_4TiOF_3 under a milder alkaline environment as low as 1 M NaOH, rather than conventional treatment of TiO_2 in 10 M NaOH, which could be made sense on the TiO_6 octahedra arrangement. The as-prepared TiO_2 nanocrystals with exposed {001} facets exhibit high photocatalytic activity and sedimentation rate as compared to commercial TiO_2. Further doping or ion-exchange, the newly prepared TiO_2 nanocrystals will show potential applications in environment.

Introduction

Titania (TiO_2) nanoparticles and titanate nanotubes have received the very same particular attention among the TiO_2-based nanomaterials for unique applications in photocatalysis, photovoltaics and gas sensing.[1-8] These applications often require controlling the morphology (size and shape) with specific phases or surface properties of the nanostructures. At atomic structural level, TiO_2 in three polymorphs (anatase, brookite and rutile) are built of TiO_6 octahedra in terms of atomic ordering.[9-11] Further investigations on local structures of different morphologies show that the atomic ordering in dense-filled titania nanoparticles are built of 3D network of TiO_6 octahedra, similar to that of TiO_2 polymorphs, whereas hollowing titanate nanotubes are arranged in corrugated layers of TiO_6 octahedra. That is, morphologies of nanostructured titania and titanate materials can be integrated in atomic ordering of TiO_6 octahedra. In principle, the common structural feature determines that the precursor phase involving TiO_6 octahedra or similar building units may be converted to any of the titania and titanate forms in a controllable way. Hence, it would be more precise to design and control the desired morphologies by altering atomic arrangement of an appropriate precursor involving topotactical transformations. Up to now, the related syntheses based on this strategy and simultaneously controlling morphologies and surface properties is rather limited.[12-14]

Recent studies reveal NH_4TiOF_3 to be a promising candidate for tailoring the TiO_2-based nanostructures of a diverse nature.[15-18] Its orthorhombic crystal structure consists of layers of distorted corner sharing TiF_2O_4 octahedra between which NH_4^+ are inserted.[19] Moreover, NH_4TiOF_3 and anatase TiO_2 share the similar atomic arrangement with minimum lattice mismatch (0.02%) in {001} planes (Fig. S1).[19] In this study, utilizing H_3BO_3 as F scavenger, NH_4TiOF_3 with exposed {001} facets enable topotactically production of anatase TiO_2 with retainable {001} facets, which are of highly energetic and chemical reactive among anatase surfaces.[7, 20-29] These so-called high-energy facets make it an active research topic in very recent titania chemistry. The as-prepared titania nanocrystals (NCs) with exposed {001} facets exhibit high photocatalytic activity. On the other hand, as a layered material, NH_4TiOF_3 has ability to form nanotubes.[30] However, no attempt has been made so far to predict and synthesize nanotubes based NH_4TiOF_3 layered structure. Herein, titanate nanotubes (NTs) can be formed by extraction of NH_4^+ and F from NH_4TiOF_3 under a milder alkaline environment as low as 1 M NaOH, rather than conventional treatment of TiO_2 in 10 M NaOH.

Experimental

[a] Key Lab for Advanced Materials and Institute of Fine Chemicals, East China University of Science and Technology, Shanghai 200237, China. E-mail: mingyangxing@ecust.edu.cn; jlzhang@ecust.edu

† Electronic Supplementary Information (ESI) available: A (001) projection of the atomic structure of NH_4TiOF_3 and TiO_2, equilibrium shape of the anatase TiO_2 crystal, XRD patterns of the NCs at different temperatures, XRD patterns of the samples with different reaction durations and NaOH concentrations. This material is available free of charge via the Internet at http://pubs.acs.org. See DOI: 10.1039/x0xx00000x

‡ Penghua Wang and Qiuying Yi contributed equally to this work.

Chemicals

All chemicals were used as received: titanium (IV) butoxide (TBOT, 97%), ammonium acetate (CH_3COONH_4), dehydrated ethanol, H_3BO_3, NaOH pellets and Methyl Orange (MO) were AR grade purchased from Sinopharm Chemical Reagent Co., Ltd., Ionic liquid (IL) 1-butyl-3-methylimidazolium tetrafluoroborate ($[bmim]^+[BF_4]^-$) from Chemer Chemical Co., Ltd. (Hangzhou, China)，Degussa P25 from Shanghai Haiyi Co., Ltd, which consists of about 30% rutile and 70% anatase and a primary particle size of about 20 nm, commercially available pure anatase from Shanghai Caiyu Co., Ltd and the average primary particle size of *ca.* 20 nm.

Synthesis of NH_4TiOF_3 mesocrystals

In a typical procedure, a transparent TBOT solution was formed by dissolving 1.5 mL of TBOT into 20 mL of dehydrated ethanol under dry atmosphere to obtain solution A. Then, 0.5 g of CH_3COONH_4 was dissolved into 15 mL of dehydrated ethanol to form clear solution to obtain solution B. Solution A was mixed with solution B at the room temperature. After that, 2 mL of $[bmim]^+[BF_4]^-$ was then added to the above mixture under vigorous stirring. The obtained transparent solution was diluted with 30 mL of dehydrated ethanol and transferred to 100 mL of Teflon-lined autoclave. Afterwards, the autoclave was sealed and maintained at 120 °C for 12 h and cool to room temperature naturally. A white precipitate was collected by decantation, centrifugation and then washed with distilled water and dehydrated ethanol (twice), and dried under vacuum at 60 °C for 8 h.

Synthesis of TiO_2 nanocrystals

In a typical procedure, 0.2 g of as-prepared NH_4TiOF_3 mesocrystals were dispersed in a 50 mL of aqueous H_3BO_3 solution (0.5 M) by vigorous stirring and then transferred to a Teflon-lined autoclave. The autoclave was sealed and maintained at 180 °C for 12 h and cool to room temperature naturally. A white precipitate was collected by decantation, centrifugation and then washed with distilled water and dehydrated ethanol twice, and dried under vacuum at 60 °C for 8 h.

Synthesis of titanate nanotubes

In a typical procedure, 0.2 g of as-prepared NH_4TiOF_3 mesocrystals were dispersed in a 50 mL of aqueous NaOH solution (1M) by vigorous stirring and then transferred to a Teflon-lined autoclave. The autoclave was sealed and maintained at 180 °C for 48 h and cool to room temperature naturally. A white precipitate was isolated upon decanting, centrifugation and then washed repeatedly with copious amounts (100 to 200 mL) of distilled water until the pH value close to 8.

Photocatalytic Test

Experiments of photocatalysis in the degradation of MO (50 mL, 20 mg/L) were carried out in XPA-7 photochemical reactor (Xujiang eletromechanical Plant, Nanjing) in the presence of the photocatalysts (1 g/L) by UV light irradiation equipped with a 300 W high pressure mercury lamp. At given irradiation time intervals, 2 mL aliquots were sampled and centrifuged to remove the residual photocatalysts particles. The degree of degradation was obtained at 464 nm by time intervals detection on Varian. Cary 100.

Characterization

X-ray diffraction (XRD) measurements were carried out with a Rigaku D/MAX-2550 with CuKα radiation (40 kV, 100mA). The SEM samples were mounted onto conductive carbon tapes and then attached onto the brass stubs, followed by gold sputtering. SEM images were taken by a JEOL JSM-6460 at 15 kV. The TEM Samples were generally prepared by ultrasonically dispersing in ethanol and depositing a drop of suspension samples onto a 300-mesh Cu grid coated with a carbon film (a holey carbon film for titanate nanotubes observation). Low magnification TEM images were taken on a JEOL JEM-2011 at 120 kV. HRTEM images and SAED patterns were obtained on a JEOL JEM-2100F at 200 kV. The instrument employed for X-ray photoelectron spectrum (XPS) studies was a Perkin-Elmer PHI 5000C ESCA system with Al Kα radiation operated at 250 W. The shift of the binding energy due to relative surface charging was corrected using the C1s level at 284.4 eV as an internal standard.

Results and discussion

We used an environmentally friendly ionic liquid (IL), 1-butyl-3-methylimidazolium tetrafluoroborate, as reaction media for the synthesis of NH_4TiOF_3 precursor. Here, the role of ionic liquid can be two-fold: one is a strong alignment matrix for favoring 2D lamellar structures,[31] and the other is creating F rich environment (BF_4^- group) to stabilize {001} facets by greatly reducing the surface energy.[6, 32] The XRD pattern of the samples in Fig. 1a shows sharp (002) diffraction peak of NH_4TiOF_3 and the intensity ratio of (002)/(020) is much higher than the reference value (5.5 vs. 1.6).[33] The SEM and TEM images (nanoflake) in Fig. 1b and c exhibit sheet-like morphology with a dimension of several μms. The HRTEM image has a lattice spacing of 0.38 nm, corresponding to {020} planes (Fig. 1d). The SAED patterns show typical mesocrystals diffraction spots (single-crystal like with minor distortion), which can be indexed to the [001] zone.[15, 18, 34, 35] Collectively, above observations confirm that the surfaces of highly-ordered NH_4TiOF_3 with dominated {002} planes are oriented parallel to {001} facets.

Anatase TiO_2 NCs with high-energy facets are formed by hydrothermal treatment of NH_4TiOF_3 mesocrystals in H_3BO_3 media at 180 °C for 12 h. Most of NCs of ca. 20 nm displayed truncated bipyramid shape and fewer were cubic shape under low-magnification TEM observation (Fig. 2a). The HRTEM image in Fig. 2b, the lattice spacing of 0.35 nm and 0.47 nm corresponds to the {101} planes and {002} planes,[36] respectively, indicating that the top/bottom surface exposed by truncation is bound by {001} facets. The measured angel of 68.3° is identical to the theoretical value for the angle between

the {001} and {101} facets.[21, 36] Fig. 2c shows two sets of lattice spacing of 0.35 nm corresponding to enclosed {101} planes with a measured angel of 97.9°, which is consistent with our calculation result for the interfacial angle between adjacent {101} facets (Fig. S2). These two kinds of 2D lattice fringes in Fig. 2b, c, fit well with the simulated model and interfacial angel viewed along a and c-directions in Fig. 2d. Therefore, we suppose most of the NCs lay in copper grid along the [001] direction and fewer stood normal to [001] direction as well. Additionally, this simulated shape is identical to the equilibrium shape of anatase crystals according to the Wulff construction.[37]

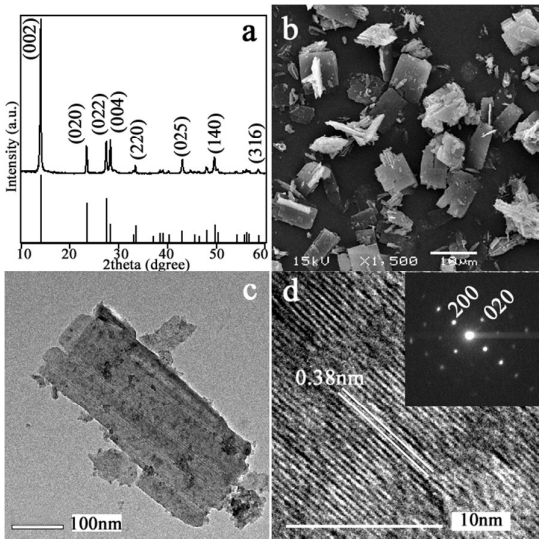

Fig. 1 (a) XRD patterns, (b) SEM image, (c, d) TEM and HRTEM images of a nanoflake falling off the mesocrystals after ultrasonic treatment. The inset is corresponding SAED pattern of a zone (200 × 200 nm^2).

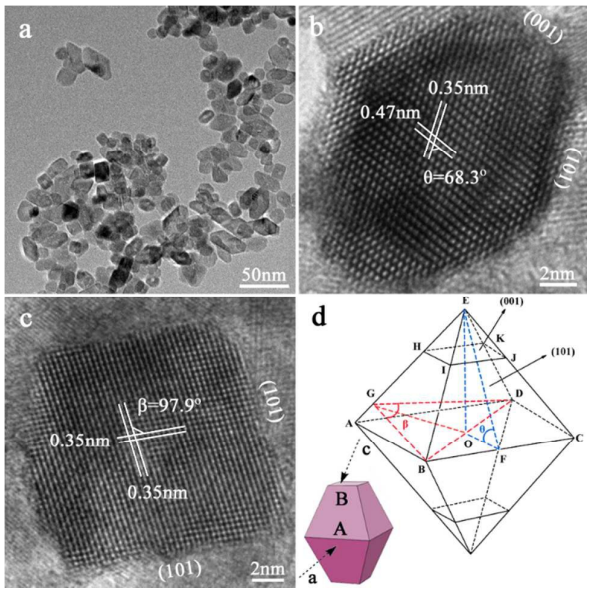

Fig. 2 (a) TEM image, (b, c) HRTEM images of the TiO_2 NCs, (d) simulated model of NCs (B/A define the degree of truncation) and interfacial angel between {001} and {101} facets (θ = 68.3°), and adjacent {101} facets (β = 97.9°).

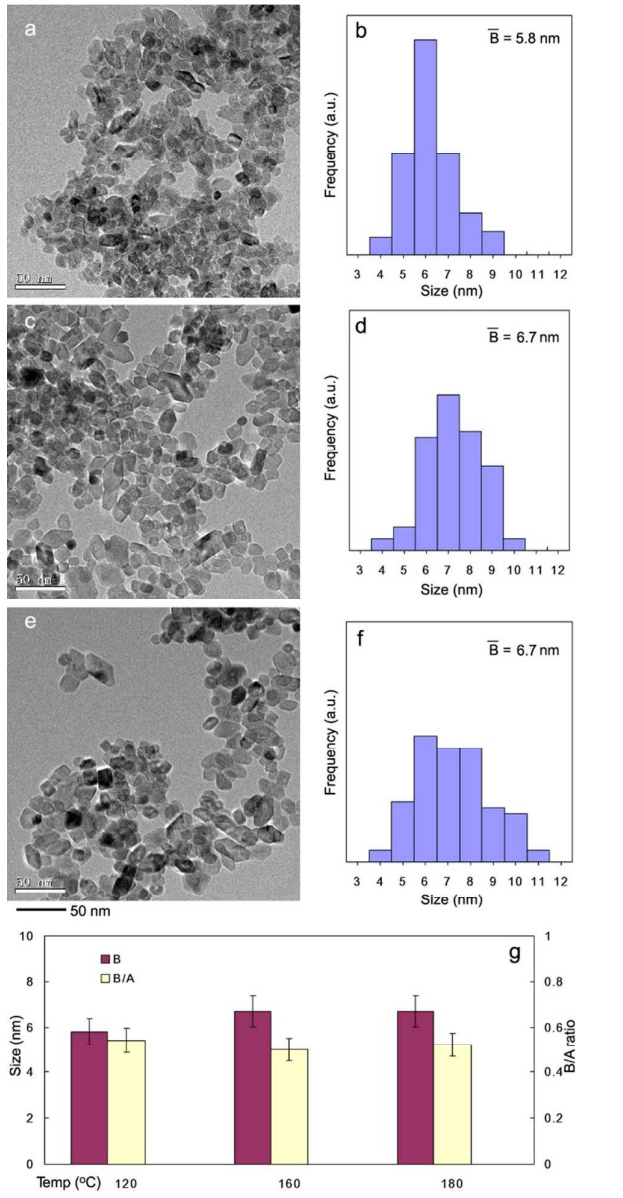

Fig. 3 TEM images and corresponding size-histograms of NCs at (a, b) 120 °C, (c, d) 160 °C and (e, f) 180 °C. (g) The dependence of average size B and aspect ratio B/A at different temperatures. The average size of B̄ increases slightly in terms of temperatures, while value of B/A keeps a constant of ca.0.50, indicating the NCs keep their degree of truncation at different temperatures.[40]

The ratio of {001} facets to total surface area can be calculated from the degree of truncation (the aspect ratio of B/A, as shown in Fig. S2). Further adjusting the temperature, the B/A value keep constant of ca. 0.50 and hence the percentage of {001} facets on the surface can be well controlled to be ca. 11% (Fig. 3). With the increase of the temperature, the nanocrystal size has a little increase (Fig. 3a-f and Table S1), but the dispersion and (001) facets percentage of NCs have no any decrease. The NCs with higher specific surface areas are expected to have a considerable total area of exposed {001} facets as compared to the micrometer-sized

TiO_2 reported in previous studies.[24, 26, 38-40] For instance, Wang and his co-workers have successfully prepared the anatase TiO_2 mesocrystals with a Wulff construction of nearly 100% exposed {101} facets and employed it in the dye-sensitized solar cells.[38] They found the high light adsorbance

, high reflectance and low transmittance in the visible region of TiO_2 mesocrystals is mainly due to the unique nearly 100% exposed {101} facets. And this mesocrystals were used as a scattering layer in the P25-based DSSCs. Differently, in our investigation here, 11% {001} facets exposed on TiO_2 nanocrystals is expected to have a high photocatalytic activity. The XRD patterns (Fig. S3) exhibit well-defined peaks assigned to pure anatase TiO_2 (JCPDS 21-2172). The average crystalline size of NCs estimated from (101) and (004) diffraction peaks by Scherrer formula indicates that the growth is hindered along [001] direction, whereas a tendency of growth was observed along [101] direction. These facts reveal that F rich environment (BF_4^- formed by H_3BO_3) on the crystal surface greatly reduce the surface energy of {001} facets, making them more stable than {101} facets.[32] The XPS spectrum of F1s core electrons for the TiO_2 NCs is shown in Fig. S4. The measured binding energy is only 684.4 eV, which is a typical value for fluorated TiO_2 systems such as the surface Ti–F species.[27] This result indicates that there are some F on the crystal surface which exhibits a high degree of truncation. In each case, the size dimension of the NCs strongly relates to the parent NH_4TiOF_3 (Table. S1). Along [001] direction, TiO_2 has greater atom density than NH_4TiOF_3 and thus size shrinkage occurs on topotactic conversion.[15, 33]

Fig. 4 shows typical TEM and HRTEM images of the NTs produced by the alkali hydrothermal treatment of NH_4TiOF_3 precursor (1 M NaOH, 180 °C for 48 h). The as-prepared NTs are 20-30 nm in outer diameter and several hundred nanometers in length. Both the axial and radial cross-sections of the NTs have a multiwall morphology (6-10 layers) and the distance of interlayer is ca. 0.8 nm, smaller than the corresponding d spacing of 0.99 nm from the XRD pattern (2θ = 8.9°, Fig. S5) due to the dehydration of the samples under high vacuum during the TEM observations.[41, 42] As the reaction time and alkali concentration increasing, the XRD patterns show characteristic of titanate and the TEM images exhibit morphology evolution from 2D nanosheets to 1D nanotubes and nanowires (Fig. 5a-c and Table 1), suggesting that the NTs were formed by scrolling of the lamellar precursor (i.e. titanate nanosheets). At higher NaOH concentration, nanosheets favor to form nanowires instead of rolling into NTs (Fig. 5c and e).[43] A scrolling sequence viewed via radial cross-section were also deliberately recorded (Fig. 5d-f and Table 1), showing the degree of scrolling with prolonged durations (1 M NaOH, 180 °C). Traditionally, onset of analogous scrolling process is slow dissolution of raw TiO_2 under alkaline conditions, accompanied by exfoliation of the titanate nanosheets.[43] In the case of sheet-like NH_4TiOF_3, the lamellar structure makes it reduce the conversion energy towards the lamellar titanate counterparts with negligible morphology changes. In a word, with the increase of reaction time, the titanate nanosheets gradually become scrolling to obtain the titanate nanotubes, and too high NaOH concentration is beneficial to the generation of nanowires instead of nanotubes.

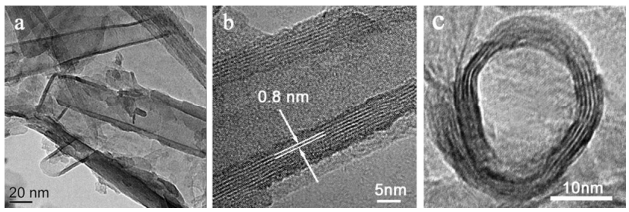

Fig. 4 (a) TEM image of the nanotubes, (b, c) HRTEM images of the individual nanotube viewed via axial and radial cross-sections.

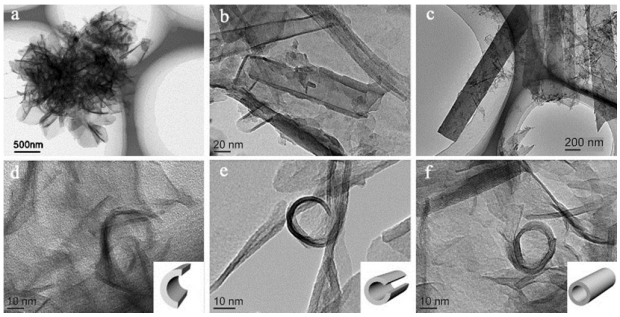

Fig. 5 Morphology evolution of the samples as (a-c) nanosheets, nanotubes and nanowires, respectively; (d-f) radial cross-section view of the scrolling samples on reaction time. Insets are the corresponding models, indicating that the tubes may probably be formed by scrolling of multilayer nanosheets. All the samples are prepared at 180 °C. The experimental conditions are listed below in Table 1.

A common structural feature of NH_4TiOF_3 and anatase is depicted by similar building units of corner-shared TiF_2O_4 and TiO_6 octahedra, where are rendered in green (Fig. 6a, b). As mentioned above, the atoms of anatase along c axis ([001] direction) is denser than that of NH_4TiOF_3, indicating that the conversion undergoes controlled stacking of units and slight rearrangement within layers.[9-11] Likewise, we propose the titanate to an orthorhombic lepidocrocite-type based on similar atomic ordering between NH_4TiOF_3 and titanate layered structures involving a controlled stacking and shearing (Fig. 6c, d).[13, 41] Thus, the conversion between these two orthorhombic structures occurs under milder alkaline conditions with relatively small structural rearrangement.

Table 1. The corresponding experimental conditions in Fig. 5.

Fig.	NaOH concentrations	Reaction Durations
a	1 M	18 h
b	1 M	48 h
c	3 M	30 h
d	1 M	18 h
e	1 M	30 h
f	1 M	48 h

*Note that the samples prepared with 2 M NaOH at 180 °C for 30 h is a mixture of nanotubes and nanowires, which is not shown here as typical motifs for further discussions.

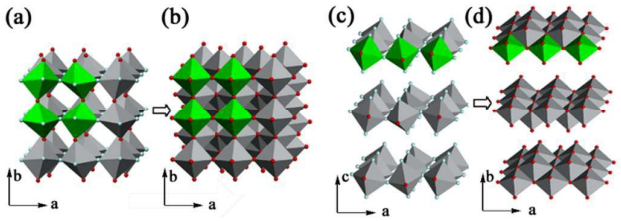

Fig. 6 Structure models of (a-b) NH_4TiOF_3 vs. anatase, (c-d) NH_4TiOF_3 vs. titanate. The similar building units of are rendered in green.

The as-prepared NCs with exposed {001} facets exhibit high photocatalytic activity. To reduce the size effect, our NCs, Degussa P25 and commercial anatase used here for comparison are similar in size of ca. 20 nm. The low adsorption capacities of MO on different samples confirms that the photo-degradation results are not influenced by an adsorption process (Fig. 7a). The NCs could degrade methyl orange (MO) to zero level and thus exhibited enhanced activity relative to that of another two commercial samples (Fig. 7b). The as-prepared NTs without further doping or ion-exchange exhibited minimal or no catalytic activity (not shown), which may be attributed to either low crystallinity or impurities of sodium.[43] The photograph of the degradation solution after irradiation under the UV light for 60 min also indicates the excellent photocatalytic activity of NCs for the degradation of MO. Compared to the solution of CA with a pale yellow color, the solution included NCs powders displays a relative transparent appearance (Fig. 7c). Additionally, we also found that our NCs were readily separated from water by sedimentation for 2 h, while Degussa P25 and commercial anatase kept unclear (Fig. 7d). Herein, due to the high surface energy, the NCs tend to aggregate and settle down. Hence, the resulting low separation cost, combined with the high photocatalytic activity, is of great significance for the environmental and industrial applications.[14, 44-46]

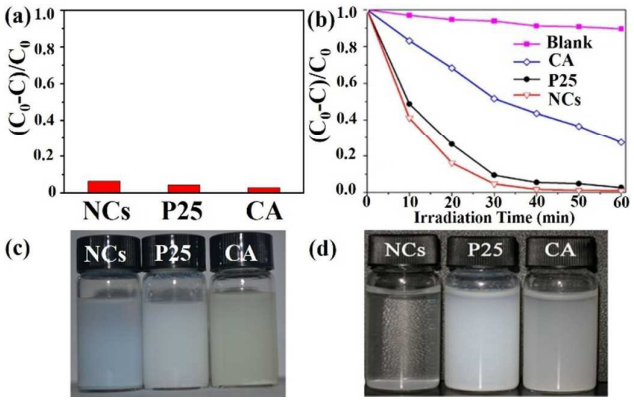

Fig. 7 (a) Adsorption capacities of MO on different samples. (b) Photocatalytic test of the samples on degradation of MO with blank, commercial anatase (denoted as CA), P25 and TiO_2 NCs (denoted as NCs). (c) Photograph of the degradation solution after irradiation under the UV light for 60 min. (d) Sedimentation for 2 h in aqueous suspensions of the samples.

Conclusions

In summary, we have demonstrated a rational conversion from an IL-mediated NH_4TiOF_3 mesocrystal to TiO_2-based nanostructures. The as-prepared titania NCs with exposed {001} facets exhibit high photocatalysis activity and sedimentation rate as compared to commercial TiO_2, which can be utilized in environmental and industrial applications. Further doping or ion-exchange, the newly prepared NTs will show potential applications. Moreover, as mesocrystal and other new nano-objects recently emerged,[47, 48] the present work will stimulate further understanding and designing the morphology of multiscale nanomaterials based on atomic arrangement.

Acknowledgements

This work has been supported by National Nature Science Foundation of China (21203062, 21377038, 21173077, 21237003), the National Basic Research Program of China (973 Program, 2013CB632403), the Research Fund for the Doctoral Program of Higher Education (20120074130001), the Fundamental Research Funds for the Central Universities (22A201514021), and sponsored by "Chenguang Program" supported by Shanghai Education Development Foundation and Shanghai Municipal Education Commission (14CG30).

Notes and references

1. X. Chen and S. S. Mao, *Chem. Rev.*, 2007, **107**, 2891-2959.
2. D. V. Bavykin, J. M. Friedrich and F. C. Walsh, *Adv. Mater.*, 2006, **18**, 2807-2824.
3. B. Qiu, M. Xing and J. Zhang, *J. Am. Chem. Soc.*, 2014, **136**, 5852-5855.
4. V. Etacheri, G. Michlits, M. K. Seery, S. J. Hinder and S. C. Pillai, *ACS Appl. Mater. Interfaces*, 2013, **5**, 1663-1672.
5. T. Leshuk, R. Parviz, P. Everett, H. Krishnakumar, R. A. Varin and F. Gu, *ACS Appl. Mater. Interfaces*, 2013, **5**, 1892-1895.
6. S. Yu, B. Liu, Q. Wang, Y. Gao, Y. Shi, X. Feng, X. An, L. Liu and J. Zhang, *ACS Appl. Mater. Interfaces*, 2014, **6**, 10283-10295.
7. Q. Xiang, J. Yu and M. Jaroniec, *Phys. Chem. Chem. Phys.*, 2011, **13**, 4853-4861.
8. J. Yu, P. Zhou and Q. Li, *Phys. Chem. Chem. Phys.*, 2013, **15**, 12040-12047.
9. M. Gateshki, S. Yin, Y. Ren and V. Petkov, *Chem. Mater.*, 2007, **19**, 2512-2518.
10. F. Alvarez-Ramirez and Y. Ruiz-Morales, *Chem. Mater.*, 2007, **19**, 2947-2959.
11. S. K. Pradhan, Y. Mao, S. S. Wong, P. Chupas and V. Petkov, *Chem. Mater.*, 2007, **19**, 6180-6186.
12. S. J. L. Billinge and I. Levin, *Science*, 2007, **316**, 561-565.
13. Y. Mao and S. S. Wong, *J. Am. Chem. Soc.*, 2006, **128**, 8217-8226.
14. H. Y. Zhu, Y. Lan, X. P. Gao, S. P. Ringer, Z. F. Zheng, D. Y. Song and J. C. Zhao, *J. Am. Chem. Soc.*, 2005, **127**, 6730-6736.
15. L. Zhou, D. Smyth-Boyle and P. O'Brien, *J. Am. Chem. Soc.*, 2008, **130**, 1309-1320.
16. X. Fu, b. Wang, C. Chen, Z. Ren, C. Fan and Z. Wang, *New J. Chem.*, 2014, **38**, 4754-4759.

17. H. Maki, Y. Okumura, H. Ikuta and M. Mizuhata, *J. Phys. Chem. C*, 2014, **118**, 11964-11974.
18. L. Zhou, J. Chen, C. Ji, L. Zhou and P. O'Brien, *CrystEngComm*, 2013, **15**, 5012-5015.
19. N. M. Laptash, I. G. Maslennikova and T. A. Kaidalova, *J. Fluorine Chem.*, 1999, **99**, 133-137.
20. M.-Y. Xing, D.-Y. Qi, J.-L. Zhang and F. Chen, *Chem. Eur. J.*, 2011, **17**, 11432-11436.
21. M. Y. Xing, B. X. Yang, H. Yu, B. Z. Tian, S. Bagwasi, J. L. Zhang and X. Q. Gong, *J. Phys. Chem. Lett.*, 2013, **4**, 3910-3917.
22. M. Y. Xing, D. Y. Qi, J. L. Zhang and F. Chen, *Chem. Eur. J.*, 2011, **17**, 11432-11436.
23. J. Pan, G. Liu, G. Q. Lu and H.-M. Cheng, *Angew. Chem. Int. Ed.*, 2011, **50**, 1-6.
24. X. Han, Q. Kuang, M. Jin, Z. Xie and L. Zheng, *J. Am. Chem. Soc.*, 2009, **131**, 3152-3153.
25. G. Liu, H. G. Yang, X. Wang, L. Cheng, J. Pan, G. Q. Lu and H.-M. Cheng, *J. Am. Chem. Soc.*, 2009, **131**, 12868-12869.
26. H. G. Yang, G. Liu, S. Z. Qiao, C. H. Sun, Y. G. Jin, S. C. Smith, J. Zou, H. M. Cheng and G. Q. Lu, *J. Am. Chem. Soc.*, 2009, **131**, 4078-4083.
27. H. G. Yang, C. H. Sun, S. Z. Qiao, J. Zou, G. Liu, S. C. Smith, H. M. Cheng and G. Q. Lu, *Nature*, 2008, **453**, 638-641.
28. W.-J. Ong, L.-L. Tan, S.-P. Chai, S.-T. Yong and A. R. Mohamed, *Nanoscale*, 2014, **6**, 1946-2008.
29. F. Wang, S. Zhang, C. Li, J. Liu, S. He, Y. Zhao, H. Yan, M. Wei, D. G. Evans and X. Duan, *RSC Adv.*, 2014, **4**, 10834-10840.
30. D. V. Bavykin, V. N. Parmon, A. A. Lapkin and F. C. Walsh, *J. Mater. Chem.*, 2004, **14**, 3370-3377.
31. M. Antonietti, D. Kuang, B. Smarsly and Y. Zhou, *Angew. Chem. Int. Ed.*, 2004, **43**, 4988-4992.
32. D. Zhang, G. Li, X. Yang and J. C. Yu, *Chem. Commun.*, 2009, 4381-4383.
33. L. Zhou, D. Smyth Boyle and P. O'Brien, *Chem. Commun.*, 2007, 144-146.
34. H. Cölfen and M. Antonietti, *Angew. Chem. Int. Ed.*, 2005, **44**, 5576-5591.
35. R.-Q. Song and H. Cölfen, *Adv. Mater.*, 2010, **22**, 1301-1330.
36. T. Y. Li, B. Z. Tian, J. L. Zhang, R. F. Dong, T. T. Wang and F. Yang, *Ind. Eng. Chem. Res.*, 2013, **52**, 6704-6712.
37. A. S. Barnard and L. A. Curtiss, *Nano Lett.*, 2005, **5**, 1261-1266.
38. Y. Zhou, X. Wang, H. Wang, Y. Song, L. Fang, N. Ye and L. Wang, *Dalton Trans.*, 2014, **43**, 4711-4719.
39. B. Wu, C. Guo, N. Zheng, Z. Xie and G. D. Stucky, *J. Am. Chem. Soc.*, 2008, **130**, 17563-17567.
40. Y. Dai, C. M. Cobley, J. Zeng, Y. Sun and Y. Xia, *Nano Lett.*, 2009, **9**, 2455-2459.
41. T. Sasaki, M. Watanabe, H. Hashizume, H. Yamada and H. Nakazawa, *J. Am. Chem. Soc.*, 1996, **118**, 8329-8335.
42. R. Ma, Y. Bando and T. Sasaki, *Chem. Phys. Lett.*, 2003, **380**, 577-582.
43. D. V. Bavykin and F. C. Walsh, *Eur. J. Inorg. Chem.*, 2009, **2009**, 977-997.
44. J. Yu, J. Low, W. Xiao, P. Zhou and M. Jaroniec, *J. Am. Chem. Soc.*, 2014, **136**, 8839-8842.
45. L. Ye, J. Mao, J. Liu, Z. Jiang, T. Peng and L. Zan, *J. Mater. Chem. A*, 2013, **1**, 10532-10537.
46. N. Roy, Y. Sohn and D. Pradhan, *ACS Nano*, 2013, **7**, 2532-2540.
47. Z. Bian, T. Tachikawa, P. Zhang, M. Fujitsuka and T. Majima, *Nat. Commun.*, 2014, **5**.
48. S. Mann, *Nat. Mater.*, 2009, **8**, 781-792.